Article

Spectroscopic Studies of a Phosphonium Ionic Liquid in Supercritical CO$_2$

Mark P. Heitz * [ORCID]**, Zackary C. Putney and Joel Campaign**

Chemistry and Biochemistry Department, The College at Brockport, State University of New York, Brockport, New York, NY 14420, USA; zputn1@brockport.edu (Z.C.P.); jcamp6@brockport.edu (J.C.)
* Correspondence: mheitz@brockport.edu; Tel.: +585-395-5586

[check for updates]

Abstract: Fluorescence spectroscopy was used to study a solution comprised of coumarin 153 (C153)+ trihexyltetradecylphosphonium bis(trifluoromethylsulfonyl)imide ($[P_{6,6,6,14}]^+$ $[Tf_2N]^-$)+ supercritical CO$_2$ (scCO$_2$). We compare the spectroscopy of C153 in neat scCO$_2$ to that of C153/scCO$_2$ with the addition of ionic liquid (IL). Excitation and emission peak frequencies of C153 in scCO$_2$ and in IL/scCO$_2$ diverged at reduced densities ($\rho_r = \rho/\rho_c$) below the CO$_2$ critical density. At low fluid density, spectral changes in the IL/scCO$_2$ solutions showed evidence that C153 experiences a very different microenvironment—one that is unlike neat scCO$_2$. The data show that the presence of IL clearly influences the C153 excitation and emission profiles. Excitation was broadened and red shifted by >2000 cm^{-1} and the presence of an additional low-energy emission component that was red shifted by ~3000 cm^{-1} was clearly visible and not observed in neat scCO$_2$. The solution heterogeneity was controlled by changing the scCO$_2$ density and at high fluid density, both the excitation and emission spectra were more similar to those in neat scCO$_2$. Steady-state anisotropy also showed that at low fluid density, the C153 emission was significantly polarized. Aggregation of C153 has been reported in the literature and this led us to hypothesize the possibility that C153 dimer (aggregation) formation may be occurring in scCO$_2$. Another possible explanation is that dye–IL aggregates may dissolve into the scCO$_2$ phase due to C153 acting as a "co-solvent" for the IL. Time-resolved intensity decay measurements yielded only slightly non-exponential decays with accompanying time constants of ~3–4 ns that were significantly shorter than the 5–6 ns time constants in neat scCO$_2$, which are suggestive of C153–IL interactions. However, these data did not conclusively support dimer formation. Pre-exponential factors of the time constants showed that almost all of the emission was due to monomeric C153.

Keywords: ionic liquid; trihexyltetradecylphosphonium bis (trifluoromethylsulfonyl) imide; supercritical fluid; carbon dioxide; time-resolved fluorescence

1. Introduction

Ionic liquid solutions (ILs) have been studied extensively in recent decades. ILs are considered to be "designer" solvents because of the ability to choose pairings of cation and anions to create a medium that is "task specific" [1] for chemical processes or reaction media. There are many review articles available that discuss the features and applications of ILs [2–5]. With respect to physical and chemical properties, ILs have attractive characteristics including non-flammability, low volatility and water miscibility, which garners attention for use as cosolvents [6–9], and in numerous applications [6–17] that include electrochemistry [18–20], organic synthesis [21,22], gas separation/supported liquid membranes (SLMs) [23,24], and catalysis [21,25]. On the whole, IL structuresshow microheterogeneity, and work has identified that nanodomains in ILs allow them to solvate both non-polar and polar solutes, which has further increased their study [11,18,19,21,23–26].

Over many years now, supercritical fluids (scf) in general, and specifically carbon dioxide (CO_2), have been studied because of their demonstrated potential as solvents for more green chemical processing [12,27]. The simplicity of tuning solvent characteristics by only changing pressure, and subsequently density, is one significant feature of the medium [28–30]. At the same time, one of the primary problems is the difficulty with which polar media can be dissolved. For CO_2 this is mainly because of its low dielectric constant [31]. One means by which the impact of this limitation has been reduced was to modify CO_2 by the addition of a few mole percent of a polar organic cosolvent such as methanol or acetone [32]. However, if the intent is to create green(er) chemical processes, then the inclusion of an organic cosolvent is somewhat counterproductive.

For nearly two decades, CO_2–IL interactions have been the focus of much research. Some examples for IL applications have been used for gas capture/solubility, e.g., CO_2 and SO_2 [33–36], catalyst recycling [27,37], and processing of nanomaterials [12]. Much of this work has focused has been heavily concentrated on 1-alkyl-3-methyl imidazolium cations ($Im_{x,1}^+$), where the alkyl chain length (x) most commonly has been C_2 to C_6 [12,27,35,37–51]. Much of this work has sought to address the phase behavior when CO_2 is dissolved in bulk ILs and then to quantify the solubility of CO_2 gas in the IL phase. In one case, CO_2 gas solubility in [C_9-imidazolium][PF_6] increased by approximately 22% in comparison to the shorter butyl chain [C_4-imidazolium][PF_6] determined from the volume increase of the liquid phase when pressure at 298 K was increased [52]. All of the recent work collectively shows that CO_2 gas is effectively captured by a bulk IL phase. Moreover, several imidazolium ILs with cation alkyl chains of C_2 to C_8 are reported not to be appreciably soluble in $scCO_2$ [53].

While much of the IL literature still focuses on the imidazolium cation, by comparison, much less attention has been given to phosphonium cations. This is beginning to change and, of the phosphonium cations, the trihexyltetradecylphosphonium cation ([$P_{6,6,6,14}$]$^+$) shown in Figure 1 has been the cation of choice [54–57]. Some time ago, we reported that a phosphonium IL was dispersed into $scCO_2$ [56]. In that work, the phase behavior of trihexyltetradecylphosphonium chloride ([$P_{6,6,6,14}$]$^+$ Cl^-) in $scCO_2$ was observed using a variable volume view cell and the data suggested that the phosphonium chloride has a solubility of up to ~7 mass% IL [56]. As part of that work, the fluorescence emission spectrum of laser dye coumarin 153 (C153), Figure 1, showed that the presence of IL had a measurable effect on the C153 emission. This observation prompted to perform a systematic study of [$P_{6,6,6,14}$]$^+$ Cl^- in $scCO_2$ [57]. In that work, we observed an unusually broad excitation spectrum at low fluid density that appeared much more similar to C153 in neat $scCO_2$ as density was increased above ρ_r (= ρ/ρ_c) ~1. Moreover, the C153 emission spectra clearly showed two distinct peaks at $\rho_r < 1$. These spectral features led us to hypothesize C153 dimer formation as a possible explanation of the observed data. Fluorescence intensity decay data yielded three time constants, which further supported the notion of C153 aggregation in the presence of IL given that the intensity decay of C153 in neat $scCO_2$ is monoexponential. This work led us to question whether the [$P_{6,6,6,14}$]$^+$ Cl^- result was anomalous or whether other [$P_{6,6,6,14}$]$^+$ ILs display the same behavior.

In this paper, we present a study in parallel to our previous work with the phosphonium chloride analog, but here report on the C153/[$P_{6,6,6,14}$]$^+$ [Tf_2N]$^-$/$scCO_2$ system. The objective of this work was to determine whether the anion paired with [$P_{6,6,6,14}$]$^+$, specifically through the use of the bis(trifluoromethylsulfonyl)imide anion, has any measurable effect on C153 fluorescence. Part of the impetus for this choice of IL was driven by previous studies of fluorinated surfactants in $scCO_2$. In the late 1980s and early 1990s, an extensive search was undertaken to find a CO_2-philic surfactant that was soluble in $scCO_2$ and, further, would form reverse micelles in $scCO_2$. Although more than 150 surfactants were tested, none formed reverse micelles except for tailor-made fluorinated surfactants [31] (and references therein). Johnston, O'Rear, and co-workers reported that fluorination of the surfactant tail(s) overcame $scCO_2$ solubility limitations because of the decrease in the Hildebrand solubility parameter, δ, and polarizability-to-volume ratio, α/υ, relative to purely hydrocarbon tail surfactants [31]. Subsequent work further demonstrated the formation of reverse micelles by solubilizing a protein (BSA) [58] and polar dyes in a $scCO_2$ continuous phase [59]. In addition, the medium has been used

to synthesize TiO_2 nanoparticles [60,61]. Clearly, fluorine has an impact on "CO_2-philicity" and thus is our reason for selecting the $[Tf_2N]^-$ anion for our work here. Both spectral and time-dependent fluorescence data from C153 in $[P_{6,6,6,14}]^+$ $[Tf_2N]^-$ /scCO_2 at 323K are reported. We selected the C153 probe both for our own internal consistency and because C153 has been extensively studied as a solvation probe by the Maroncelli group (among others) in conventional liquids and in supercritical fluids [26,28,62–64]. C153 is a nearly ideal probe of solvation primarily because the $S_0 \rightarrow S_1$ transition is not complicated by any nearby transitions [65,66]. Both experimental and computational work are in good agreement and show that the C153 spectroscopic properties make it an ideal probe of molecular solvation [62,67,68].
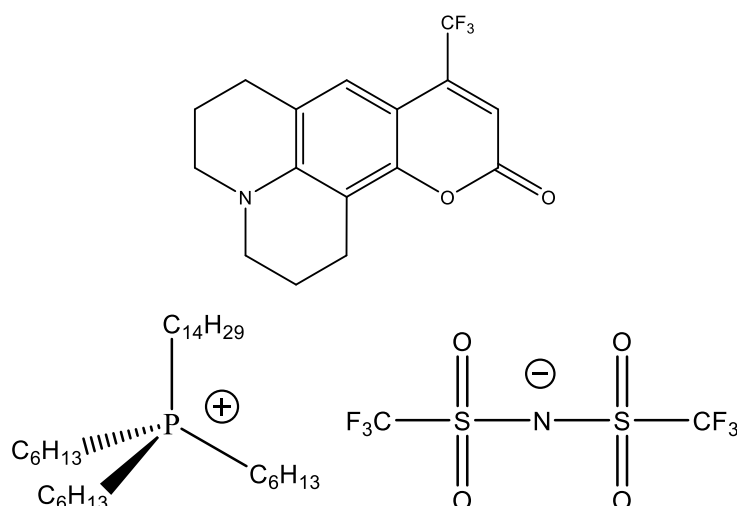

Figure 1. The top structure is the laser dye coumarin 153 (C153) and the lower structures are the ions in trihexyltetradecylphosphonium bis(trifluoromethylsulfonyl)imide $[P_{6,6,6,14}]^+$ $[Tf_2N]^-$.

2. Materials and Methods

Trihexyltetradecylphosphonium bis(trifluoromethylsulfonyl)imide ($[P_{6,6,6,14}]^+$ $[Tf_2N]^-$) was provided by Cytec Canada [69]. The IL was treated in activated carbon to remove organics and filtered through a 0.2 micron nylon mat and then dried under vacuum for 5 days at ~60 °C. The resulting IL was colorless by eye. The Karl Fischer titration method was used to assess water content at 295 K. For this, we used a C20 titrator from Mettler Toledo, Co that was fitted with a double platinum pin electrode (model DM 143-SC). Replicate measurements showed water content less than 0.015 ± 0.003 mass% water. Carbon dioxide (Scott Specialty Gases, 99.99% purity) was used as received. Isothermal properties for CO_2 were computed at 323 K using the National Institute of Standards and Technology (NIST) webbook [70]. CO_2 densities were calculate using the Span and Wagner equation-of-state (EOS) [71]. The CO_2 critical parameters are also reported on the NIST website, T_c = 304.128 K, P_c = 1070.0 psia, and ρ_c = 0.4676 g·mL^{-1}. Laser grade coumarin 153 was purchased from Exciton and used as received.

The details of the pressure apparatus have been reported previously [57] and consist of a stainless steel optical cell that uses quartz windows and Teflon®O-ring seals. All measurements were made at 323.3 K with temperature controlled with a CN76133 Omega Engineering controller unit that drove two model CIR−1031 resistive cartridge heaters. Temperature feedback from the cell was through a JMQSS−125G-6 thermocouple and was maintained to ±0.5 K. Pressure control was from an Isco Model 260D syringe pump and read using a Heise CC Dial gauge with an uncertainty of ±2 psia.

Samples were prepared by pipetting 30 µL of stock 1 mM C153 from a methanol solution into the cell and evaporating using dry nitrogen. Probe concentration in the final solution was less than 10 µM. Prior to sealing the cell, gaseous CO_2 was allowed to flow through the cell as a final purge prior closure, heating and pressuring. Fluorescence spectra were recorded with pressure varying over a

range 1070–3500 psia at 323.3 K, which equates to $\rho_r = \rho/\rho_c \sim 0.4 - 1.8$. The pressure was set to the initial value and equilibrated for 12–15 h overnight by stirring with a magnetic stirrer. During the measurements, we allotted at least a five minute equilibration period per pressure increment. Due to sample compartment size restrictions, stirring was discontinued before measurement, but the solution was further equilibrated for an additional (at least) five minutes after the cell was transferred into the instrument. The cell contents were examined visually to confirm optical transparency at all pressures. There was never any indication of a biphasic solution.

A Fluorolog-3 spectrometer from Spex (now Horiba Instrument) was used to acquire fluorescence excitation and emission spectra. The spectrometer is outfitted with a single grating excitation monochromator and a double-grating emission monochromator. Choice of instrument settings were selected to produce a spectral resolution of 2 nm. Initial calibration was done by measuring the Raman signal from distilled-deionized water. Post-acquisition blank subtraction and was performed on all spectra. Spectral uncertainties were <250 cm^{-1}. Steady-state polarization measurements were made using the instrument's Glan–Thompson polarizers. Polarizer calibration was performed using a dilute scattering solution and the resulting anisotropy was 0.990, exceeding the manufacturer's specification tolerance of >0.97. Polarization data were collected at several excitation/emission pairs: $\nu_{ex} = 27{,}397$ and 24,691 cm^{-1} with $\nu_{em} = 22{,}222$ cm^{-1} and then at $\nu_{ex} = 22{,}222$ cm^{-1} with $\nu_{em} = 19{,}608$ cm^{-1} and signal averaged 10 replicates.

For time-dependent emission, our instrument was modified to include time-correlated single photon counting (TCSPC) components, which has been previously discussed [57,72]. For these experiments, all time-resolved decay measurements were excited using a 405 nm diode laser, high output NanoLED, from Horiba. Laser output was passed through a vertical polarizer and the emission polarization was controlled by a Glan–Thompson polarizer set at "magic" angle (54.7º) for lifetime measurements. Emission wavelength selection was accomplished with the Fluorolog-3 emission monochromator and detected with an air-cooled IBH TBX-850 photomultiplier. The instrument response was measured with a dilute scattering solution that was intensity matched to the sample in a separate, identical stainless steel cell. The nominal instrument response was <200 ps. The C153 intensity decays were measured with a 7.1 ps per channel resolution. Data fitting was performed with the iterative reconvolution method as provided by the IBH DAS6 version 6.6 software. A sum-of-exponentials algorithm was used to model the intensity decay,

$$I(t) = \sum B_i \exp(-t/\tau_i) \tag{1}$$

where B_i represents pre-exponential coefficients, t is the time and τ_i represents the component lifetimes. We estimate that after reconvolution, the instrument time resolution is effectively $\sim$60 ps [57,73–75]. Fitting quality was assessed by the reduced chi-squared method (χ_r^2) with an "acceptable fit" defined as the χ_r^2 value $\sim$1.0–1.2 accompanied by the residual autocorrelations that displayed no clear systematic pattern. We imposed an "improvement threshold" for including additional lifetimes only when the resulting fits yielded at least a 10% χ_r^2 reduction with accompanied residual and autocorrelation improvement. For multi-component fitting models, we computed lifetime fractions (f_i) using

$$f_i = \frac{B_i \tau_i}{\sum_{i=1}^{n} B_i \tau_i} \tag{2}$$

with B and τ as described above. Lifetime uncertainties were $< \pm 70$ ps as determined from replicate measurements.

3. Results and Discussion

3.1. Fluorescence Excitation and Emission Spectroscopy

A set of normalized excitation and emission spectra are presented in Figure 2 for C153 in scCO$_2$ (see upper panel) and for [P$_{6,6,6,14}$]$^+$ [Tf$_2$N]$^-$/scCO$_2$ (in the lower panel) at T = 323K. The C153/scCO$_2$ excitation and emission spectra are in good agreement with previous measurements [28,57] and show a consistent red shift as scCO$_2$ density increased. The C153 spectral shapes in CO$_2$ are similar to what one observes in conventional liquid solvents that have polarities which are comparable with CO$_2$. Blank scans in neat scCO$_2$ and IL+ scCO$_2$ showed only background-level signal with no obvious spectral features in either excitation or emission. The lower panel of Figure 2 shows examples of C153-normalized excitation and emission in IL-modified scCO$_2$ at reduced densities that cover the entire density range in these measurements. What is immediately noticed is that excitation spectra of IL/scCO$_2$ at ρ_r <1 showed a completely different shape compared to that in neat scCO$_2$. The entire spectrum was shifted to lower energy (blue line, ρ_r = 0.44, centered at 24,000 cm^{-1}) and the excitation spectrum is substantially broader than the neat scCO$_2$ counterpart. The set of excitation spectra up to approximately ρ_r ~ 1 showed two distinct contributions to the excitation envelope that were never completely resolved. At the lowest few densities studied (ρ_r ~ 0.42–0.48), peak separation was not readily apparent but became noticeable at approximately ρ_r ~ 0.55. As density was further increased, the lower frequency shoulder intensity rapidly decreased and red shifted by ~1500 cm^{-1}. The diminution and red shift of the low-energy spectral component disappeared entirely above the critical density. The dotted excitation spectrum shows the last of the clearly discernable lower energy feature relative to the main peak, at ~22,500 cm^{-1}. For completeness, the set of normalized excitation spectra at ρ_r = 0.42 – 1.08 are presented in Figure S1. Excitation spectra at ρ_r > 1 for C153 in neat and IL-modified scCO$_2$ have very similar profiles in both shape and position and at the highest densities, the spectra are nearly indistinguishable; see red-dashed excitation lines at ρ_r ~ 1.7.

The emission spectra from IL solutions showed patterns similar to the excitation spectra, with a clear distinction between spectra at densities ρ_r < 1 and ρ_r > 1. At ρ_r = 0.44, the emission shows two clearly resolved peaks centered at ~20,000 cm^{-1} and ~23,000 cm^{-1}. We noted that the peak resolution was sensitive to bulk fluid density and the best resolution was achieved at low fluid density, typically ρ_r < 0.66. At higher density, the lower energy peak intensity was too weak relative to the main emission peak so that it was impossible to determine its actual position. We attempted to isolate the ~20,000 cm^{-1} emission by using excitation at 24,691 cm^{-1} (=405 nm). However, we were unable to fully isolate the lower energy emission peak. As with the spectra shown in Figure 2, the emission spectra showed the same two distinct peaks. So when using either of these two excitation energies, we observed two emission peaks at low densities, consisting of one peak that was initially at much lower energies than expected, which blue shifted with increased density, and a second peak with an energy that was more typical for C153, which red shifted with increased density. This pattern was observable up to ρ_r ~1.1 after which the emission produced the unfeatured C153 emission. Emission was examined at one additional excitation wavelength, 22,222 cm^{-1} (=450 nm), which is presented in the lower panel of Figure S2. These spectra clearly show the isolated low-energy part of the total emission.

In an effort to quantify the effects of density on the C153 emission, we computed the fluorescence intensity ratios in two ways. First, we used the intensity at the peak maximum and tracked the peak maximum as the spectrum changed with density. However, this approach was somewhat problematic because at mid and higher densities the lower energy spectral peak was at best not well-resolved, if at all identifiable. The second approach was to select a set of fixed wavelengths and use those values consistently. The values were determined to be 450 and 510 nm, which equate to 22,222 and 19,608 cm^{-1}, respectively. These values were selected by using the peak positions at the lowest and highest densities where the spectral features were most clearly observable. The results of our analyses are shown in Figure 3.
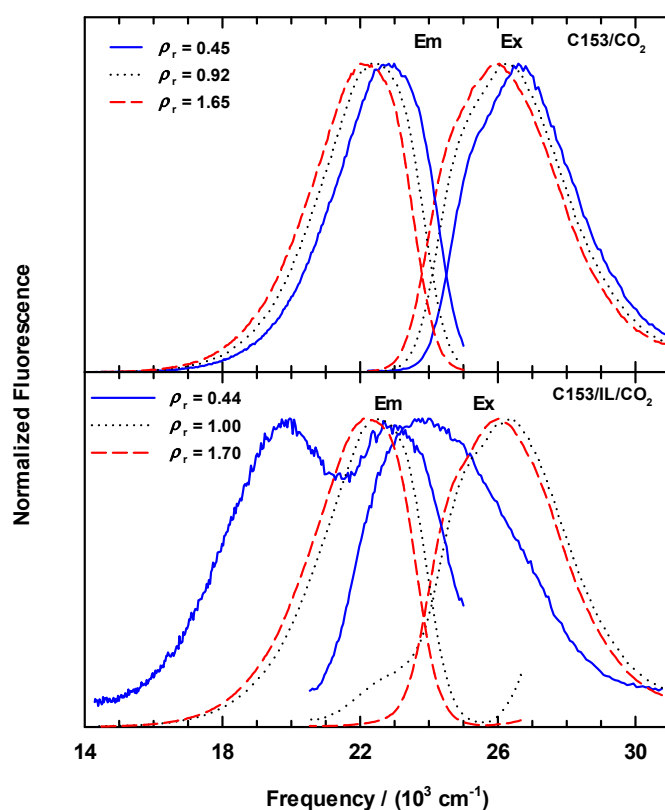
Figure 2. Excitation and emission spectra for C153 in scCO$_2$ and IL-modified scCO$_2$ at 323 K. Representative densities are chosen for values that are below, near and above the CO$_2$ critical density (solid, dotted and dashed lines, respectively). The upper panel is spectra of C153 in neat scCO$_2$. Emission spectra were measured using ν_{ex} = 27,397 cm^{-1}. The excitation spectra were measured by monitoring emission at ν_{em} = 21,053 cm^{-1}. The lower panel shows spectra for C153 in [P$_{6,6,6,14}$]$^+$ [Tf$_2$N]$^-$/scCO$_2$. Emission spectra that are centered at ~23,000 cm^{-1} were excited using 27,397 cm^{-1} photons. IL/scCO$_2$ excitation spectra at ~26,000 cm^{-1} were measured with emission set at 19,608 cm^{-1}.
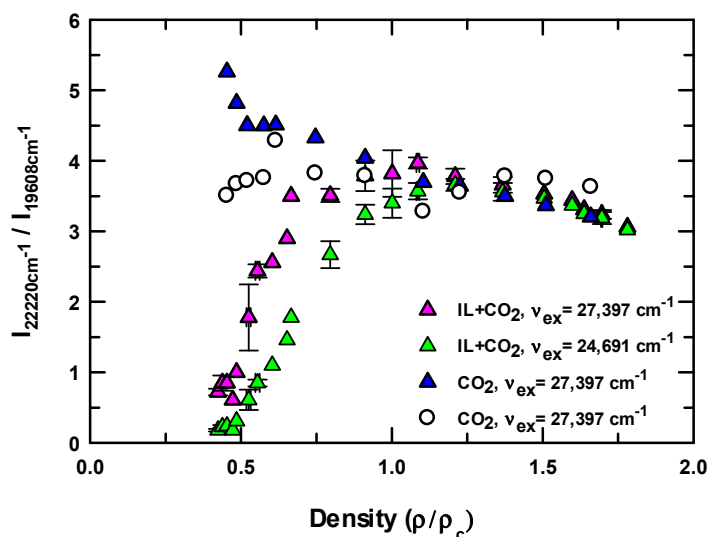

Figure 3. Computed emission intensity ratios for C153 in neat scCO$_2$ (circles and blue triangles) and [P$_{6,6,6,14}$]$^+$ [Tf$_2$N]$^-$/scCO$_2$ (pink and green triangles). Emission ratios (all triangles) are calculated from intensities at 22,222 cm^{-1} / 19608 cm^{-1} (= I$_{450nm}$/I$_{510nm}$), whereas open circles are for ratios calculated using the peak maximum value with an appropriate shift on the spectrum for the "510 nm" position. See text for details. Uncertainties are contained within the size of the symbol except for the visible error bars.

We compared these two methods using C153 in neat scCO$_2$ as the test case, shown in Figure 3 for the open circles and blue triangles. The open circles represent method 1, where the actual peak position of the ~22,222 cm^{-1} peak was used and the expected position of the 19,608 cm^{-1} peak was estimated by applying a simple wavelength shift that was determined from the difference between the actual peak maximum and 22,222 cm^{-1}. The results showed that the intensity ratio is essentially constant to within our ability to accurately determine the peak position. However, in some cases, it was difficult to determine the actual peak position because of poor resolution. The blue triangles show the results using method 2, the static wavelength approach. With increasing density, the spectrum red shifted, and the calculated ratio consistently decreased. Although method 2 does not use the actual peak position, the static wavelengths approach offered a more consistent method of calculating the ratio across all data sets, even though this introduced a slight bias in the ratio because the spectral shape changes with density. Thus, the neat CO$_2$ results served as a baseline for the ratio calculation. With IL added, the pink triangles show the calculated emission ratio using excitation at 27,397 cm^{-1} and green triangles show the ratio using excitation at 24,691 cm^{-1}. These data manifest several points. At the lowest densities, the ratio is less than unity, indicating that the 19,608 cm^{-1} contribution is greater than the 22,222 cm^{-1} contribution, which is clearly observed in the low-density spectra. Interestingly, this behavior is only observed in IL solutions, as compared with C153 in neat scCO$_2$ (blue triangles). Below ρ_r ~ 1.1, the data indicate that higher energy excitation favors the higher energy (22,222 cm^{-1}) emission peak but as with the spectra, the difference becomes negligible at high density and, more importantly, is indistinguishable from the neat CO$_2$ data. Whatever the source of the emission, the effects of IL in solution are not discernable from this measure.

All steady-state results are summarized using the first moment of the peak frequency and spectral full-width-at-half-maximum intensity (Γ). The density dependence of these data is collected in Figure 4. The upper panels show C153 excitation and emission peak positions, ν_{ex} and ν_{em} respectively, in neat scCO$_2$ ($\circ$) and with added IL in scCO$_2$ (filled symbols). With no IL, the C153 frequencies displayed a systematic shift toward lower energy with increased CO$_2$ density. Interestingly, when IL was present, the excitation peak position decreased by as much as ~3000 cm^{-1} at the lowest density in contrast with C153/scCO$_2$ with emission measured at 19,608 cm^{-1} (green triangles). On increasing the density, ν_{ex} systematically *increased* to the value observed for C153/scCO$_2$. A much weaker rise at low density was noted for ν_{ex} with emission at 22,222 cm^{-1} (blue diamonds). The C153 ν_{em} data with IL showed a similar energy change at lower density but the extent of the shift depended on the specific excitation used. Using excitation at 27,397 cm^{-1} (red diamonds), the emission showed the least change in position relative to neat CO$_2$ and correspondingly displayed the larger intensity ratio (see Figure 3, pink triangles). For all excitation wavelengths, the relatively high intensities from the lower energy emission in IL solutions contributed significantly to the weighted spectrum. In high density IL solutions, the peak positions eventually aligned with C153/scCO$_2$ values to within a few hundred wavenumbers, the limit of our experimental uncertainty. The exception is the emission when excited at 22,222 cm^{-1} (green symbols). Although we saw a small initial blue shift toward the neat CO$_2$ peak value, the peak position remained ~2500 cm^{-1} lower in energy.

Figure 4 includes the spectral width variations (Γ). C153 absorption widths in conventional liquid solvents are directly proportional to solvent polarity but the emission widths are inversely proportional [68]. Moreover, excitation spectra are broader than emission by ~20%. Here, the C153/scCO$_2$ Γ values are in general agreement with liquid results and are also consistent with previous CO$_2$ data [28]. However, Γ in IL/scCO$_2$ solutions deviated from the expected behavior. The excitation and emission widths show similar patterns with respect to increasing density in that the C153 microenvironment is significantly more heterogeneous at low density. Excitation widths in IL solution are consistently narrower than the comparable neat CO$_2$ widths. However, emission widths in IL solution are initially broader than the in CO$_2$ but are identical at high density to within-experimental uncertainty.
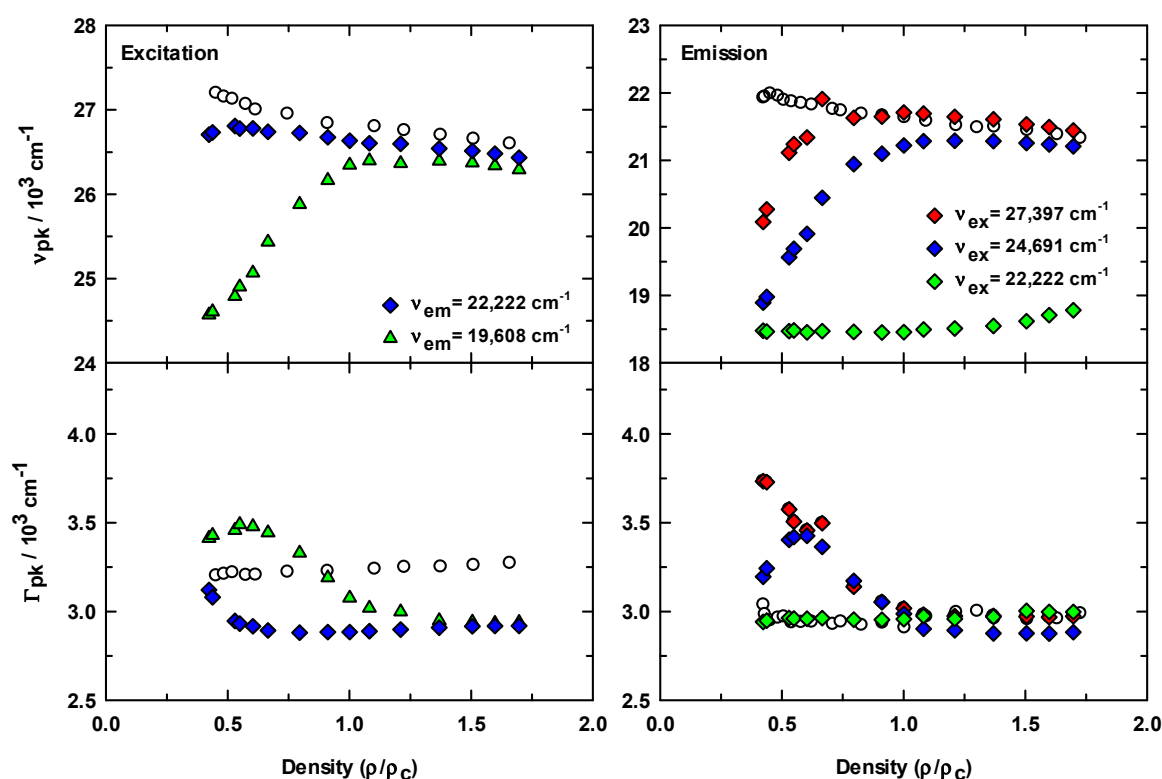
Figure 4. C153 spectral parameters in the absence (open circles) and presence (filled symbols) of $[P_{6,6,6,14}]^+$ $[Tf_2N]^-$. The upper panels show the first moments of excitation and emission frequencies. Emission data were from several excitation energies, 27,397 cm^{-1} (red symbols), 24,691 cm^{-1} (blue symbols), and 22,222 cm^{-1} (green symbols) whereas the lower panels give FWHM bandwidths. Uncertainties in peak positions are less than ~180 cm^{-1} and widths are less than 200 cm^{-1}.

The spectral data show that inclusion of IL significantly alters the C153 spectral behavior. To what then can we ascribe these observations? The signal from the $[P_{6,6,6,14}]^+$ $[Tf_2N]^-$ /scCO₂ blank was negligible at all densities, which indicates that fluorescence from the addition of IL is negligible or rather any impurities present in the IL are not extracted by scCO₂. Furthermore, all data were corrected for instrument artifacts and blank corrected to remove any spurious contributions to the observed signal. The peak frequency changes and broadened widths for $\rho_r < 1$ suggested that $[P_{6,6,6,14}]^+$ $[Tf_2N]^-$ is somehow affecting the C153 fluorescence, which was also observed with $[P_{6,6,6,14}]^+$ Cl^- [56,57]. One hypothesis that may help to explain these spectral results is that the C153 is partitioning into distinctly different solvent environments. There are at least three possible environments in the solution that could combine to produce the observed solution heterogeneity: (1) neat scCO₂; (2) an IL-rich environment; (3) a mixed IL/scCO₂ medium in which IL is somehow dispersed. Amphiphilic molecules have been reported to dissolve into supercritical fluids that resulted in the formation of a micellar environment [58–61,76,77]. While we are not implicitly suggesting that $[P_{6,6,6,14}]^+$ $[Tf_2N]^-$, is forming micelles, these surfactant reports do show that molecules similar to this IL have been solubilized in supercritical fluids. Partitioning of C153 into a microheterogeneous solution might explain the observed widths and spectral shifts, but it does not necessarily account for all spectral features. For example, while excitation and emission peaks for IL solutions red shift at $\rho_r >1$, in parallel with expected C153 behavior in scCO₂, the initial peak position and band shape of the excitation spectra at $\rho_r = 0.47$ was quite different than expected. Moreover, C153–IL interactions at low density should be blue shifted compared to a high-density spectrum, which was also inconsistent with the measured data. What else may be happening in solution? Solute–solute interactions may also be contributing to the C153 spectroscopy, especially at low fluid density where solubility is most severely limited.

Aggregation of coumarin dyes in liquid solvents has been reported for C153 [78,79], C481 [80,81], and C343 [82,83]. Pal and co-workers report blue-shifted C153 emission in ethanol for a dye concentration of ~10^{-5} M [78]. The conclusion from that work was that in ethanol C153 was able to form H-aggregates where no evidence for dimerization was reported in acetonitrile. They also reported formation of H-aggregates for C481 in ethanol and acetonitrile [81] and in binary solutions comprised of acetonitrile-water [80]. Kasha's exciton coupling theory [84,85], predicts that formation of a stacked arrangement molecular dimer that has transition dipoles aligned in parallel should shift hypsochromically (blue shift) with a simultaneous decrease in emission intensity. Conversely, J-aggregate dimerization should produce a bathochromic shift. If C153 were to aggregate because of IL influence, then the spectroscopy should be sensitive to this process. Our C153/IL/scCO$_2$ excitation spectra showed both a broadened and a red-shifted peak at low density relative to C153/scCO$_2$ (Figure 4, green symbols), which might suggest solute–solute interactions. Spectra narrowed and the peak energy increased up to ρ_r ~ 1, beyond which the spectrum systematically red shifted as expected up to the highest density. At high density, scCO$_2$ solvating power is expected to maximize and the disappearance of any solute–solute signal is not surprising. This effect could be observed if only monomers are in solution or if monomer signal is much more intense compared to any dimer signal. Density dependent solubility in supercritical fluids has long been known and many reports discuss the idea of local solvent density enhancement near to the critical point, which diminishes by a sufficient increase in density [28,86–89]. Low solubility is expected at supercritical fluid densities less than $\rho_r = 1$ where the bulk fluid density is more gas-like. Therefore, these conditions should most favor aggregation of any dissolved solute. Above the critical density, the fluid properties become more liquid-like and solubility improves. The changes we observe for C153 when IL is present mirror these effects. A second result that pointed us toward aggregation as a tentative explanation was the isolation of an additional low-energy emission band at ~19000 cm^{-1} that displayed weaker emission intensity and was undetectable at about the critical density.

Results from electronic structure calculations were used to compute anticipated C153 dimer energies [57]. From those calculations, the C153 absorption for the calculated monomer was expected at 26,810 cm^{-1}, which reasonably agreed with the low-density scCO$_2$ experimental data (Figure 2, blue line). The calculated H-aggregate spectrum showed an absorption that was correlated with the expected monomer position *and* a low-energy feature at 22,727 cm^{-1}, which is similar to what we observed experimentally (Figure S1). For completeness, we also considered J-aggregate energies but the dominant contribution to the spectrum was predicted to be at 25,445 cm^{-1} with a low-energy line predicted at 20,367 cm^{-1} that were not observed in our data. Although Kasha's model predicts that H-aggregates should be non-fluorescent because of the forbidden electronic transitions, Pal and co-workers observation of C153 fluorescent H-aggregates showed that weak, fluorescent H-aggregates did form that were red shifted relative to monomer emission [78]. They discussed the effect in terms of the vibronic coupling and rotational twisting that perturbs the C153 molecular planes so that emission, although weak, can be observed. This model appears to provide at least some insight to explain our low-density scCO$_2$ data.

Finally, an equally plausible explanation could also be based on the interactions between C153 and IL, with the C153 acting as a sort of "co-solvent" such that a dye–IL aggregate is present in the scCO$_2$ phase. While we can conjecture about all of these various possibilities, it still remains that the exact nature of the solution microheterogeneity that gives rise to our observations cannot be inferred directly from these measurements.

3.2. Steady-State Anisotropy

Fluorescence depolarization measures the rotational mobility of a dissolved fluorophore as described by Perrin [90],

$$r = \frac{r_0}{\left(1 + \frac{\tau RT}{\eta V}\right)} \tag{3}$$

where r_0 is the limiting anisotropy value, τ is the excited-state fluorescence lifetime, η is the solution viscosity, and V is the fluorophore hydrodynamic radius derived from the fluorophore size and shape. From Equation (1), depending on the known and measured parameters, the anisotropy data can be used to either determine molecular size and shape parameters or the solution viscosity if molecular parameters are already known. Thus, in these experiments, we expect that the solution anisotropy should be able to reveal direct information about C153 and its mobility characteristics and thus help to test our dimerization hypothesis. Before discussing the results, it is useful to calculate the expected anisotropy values. As a simple anisotropy prediction, we calculated values using the bulk $scCO_2$ viscosity [71], excited-state lifetime of 3 ns (see next section), C153 molecular volume of 246 $Å^3$ [72], and limiting anisotropy of 0.375 [91]. The values ranged from 0.0001 to 0.0006 at $\rho_r = 1.8$ for a C153 monomer and only up to 0.0011 for a dimer (= 2x monomer volume with no further corrections).

Figure 5 presents the measured anisotropy using several excitation/emission pairs to probe the C153 fluorescence response. As mentioned, the monomer emission is presumed to be at ~22,222 cm^{-1} (blue symbols) as determined by C153 in neat $scCO_2$ and at high density in the IL + $scCO_2$ solution and the dimer emission at 19,608 cm^{-1} (green symbols) using the low-density data. Monomer anisotropy was measured by exciting with 27,397 cm^{-1} (blue inverted triangles) and 24,691 cm^{-1} (blue squares). The low-density results show substantial anisotropy, as large as 0.1 for excitation at 27,397 cm^{-1} and 0.33 for excitation at 24,691 cm^{-1}—both of which rapidly decreased as density was increased. Similar results are observed for these two excitation energies when emission is measured at 19,608 cm^{-1} (green inverted triangles and squares). Of note for these data is that at low density, the anisotropy is unexpectedly large, but becomes unmeasurable above $\rho_r \sim 0.7$. However, what is particularly interesting in these data are the results when using excitation at 22,222 cm^{-1} with emission at 19,608 cm^{-1} (green circles). Presumably, under these spectroscopic conditions, we are directly exciting the C153 dimer—the anisotropy of which surprisingly persisted over nearly the entire range of density.
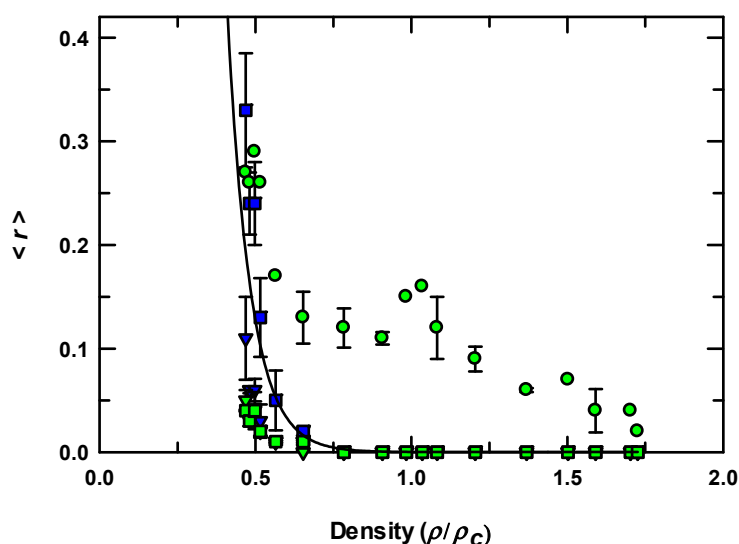

Figure 5. Density dependence of the anisotropy of C153 in $[P_{6,6,6,14}]^+$ $[Tf_2N]^-/scCO_2$. Blue symbols show data acquired with emission fixed at 22,222 cm^{-1}, whereas green symbols are the anisotropy with emission at 19,608 cm^{-1}. Excitation was varied for each emission using 27,397 cm^{-1} (inverted triangles), 24,691 cm^{-1} (squares), and 22,222 cm^{-1} (circles). Uncertainties are contained within the size of the symbol except for where there are visible error bars.

Increased anisotropy suggests that, from a mobility perspective, C153 experiences a more restrictive environment through either physical constraints or intermolecular interactions or both. Considering the current context, there are several physical phenomena that would support this observed behavior: (1) local density augmentation of neat $scCO_2$ about C153 [28]; (2) the presence of IL in $scCO_2$ that forms

a dispersed type phase; (3) C153 dimer formation; (4) C153/IL association that has been dissolved into the scCO$_2$ phase. Local density augmentation and the presence of IL could effectively increase the local viscosity about C153, thereby decreasing its mobility. Enhanced local scCO$_2$ density alone is the least likely of these three possibilities because the effects from CO$_2$ augmentation for C153 in neat scCO$_2$ is at best only a factor of 4 larger at ρ_r ~ 0.5 than ρ_r ~ 1.8 at 308K (T_r ~1.02) [28]. In addition, at 323 K, the higher temperature also further reduces the augmentation effects. Dimer (aggregate) formation increases the volume of the rotating species, which also slows rotational motion. However, the volume change alone if considering only C153 dimerization is insufficient to account completely for the observed anisotropy. Therefore, we are left with the only other contribution—the presumption that somehow the IL is entering solution is occurring. Using Equation (1), we estimated the solution viscosity required to produce the observed low-density anisotropy. Using the Perrin equation, we estimated first the viscosity and then the molecular volume that would be required to produce $<r>$ = 0.1. First, using the C153 monomer volume of 246 Å^3 [72], we estimated the solution viscosity to be ~25 mPa·s, and if we simply double the volume, then the estimated solution viscosity for a C153 dimer is ~12 mPa·s. Given that the neat IL has a viscosity of 277 mPa·s at 298K [26], and guessing a value of 100 mPa·s to account for the experimental temperature of 323K, a dilute IL solution could create the observed anisotropy effect. On the other hand, if we only use the ρ_r = 1 scCO$_2$ viscosity and compute the molecular radius of the rotating species assuming a spherical shape then we find that the radius is a 10x larger than the monomer size. However, a molecular dimer does not have 10 times the radius of the monomer. While these measurements alone do not confirm any specific underlying interactions, the spectroscopic and anisotropy data do show that the chemical environment about C153 is clearly different than in neat scCO$_2$ alone. From the very early stages of work with ILs and scCO$_2$, it has been reported that IL does not appreciably dissolve into bulk scCO$_2$ and for [bmim][PF$_6$] the solubility was 5x10^{-7} as assessed by UV-Vis spectroscopy [53]. That work also included five other imidazolium ILs and the same conclusion was reached for each of those ILs. However, here we are using fluorescence from C153 (a laser dye) to measure the effect of [P$_{6,6,6,14}$]$^+$ [Tf$_2$N]$^-$, and fluorescence detection is orders of magnitude more sensitive than absorbance. In addition, [P$_{6,6,6,14}$]$^+$ [Tf$_2$N]$^-$ is a wholly different type of IL and thus the interactions between IL and CO$_2$ will be necessarily different. Thus, there is no reason to expect that our results should be so similar to the imidazolium IL results. Importantly, a recent report by Sivaraman and co-workers using a tetraalkylammonium IL, similar to the phosphonium used here, did show appreciable solubility, on the order of (0.5 – 12.7) x 10^{-5} in neat scCO$_2$ at 313, 323, and 333K over a pressure range of 10–30 MPa [92]. It is interesting to note that only after many attempts to show surfactant dissolution in CO$_2$, only a few designer fluorinated surfactants were shown to appreciably dissolve in scCO$_2$ [31,58,59,93,94]. These works showed the importance of molecular considerations and structural motifs when considering interactions with scCO$_2$.

3.3. Time-Resolved Spectroscopy

While our spectroscopy and anisotropy data seem to hint at C153 aggregation, the inclusion of time-resolved intensity decay measurements also can be used to detect multiple emitting species [73–75,95]. Thus, if dimers are present in solution, we expect that multiple time constants should be needed to describe the excited-state intensity decay. In our C153/[P$_{6,6,6,14}$]$^+$ Cl$^-$/scCO$_2$ work, we noted that three time constants were needed to fit the measured intensity decays [57]. Here, we present intensity decays and residuals for C153/scCO$_2$ and C153 in [P$_{6,6,6,14}$]$^+$ [Tf$_2$N]$^-$/scCO$_2$ in Figures 6 and 7, respectively. The C153/scCO$_2$ decays were measured at ρ_r = 0.571 ("a", blue traces) and ρ_r = 1.659 ("b", green traces). Best fits were to a double exponential decay model (χ_r^2 = 1.05 for trace "a" in Figure 6) that resulted when a short time constant (< 70 ps) was added to the fit. This short time constant was always required to achieve the best fits, but the contribution was quite small at < 0.2%. We assigned this time constant to scattered photons. Thus, the data suggested that a single time constant adequately described the C153 emission. The longer lifetime component ranged between 6.85 and 5.17 ns at ρ_r = 0.571 and ρ_r = 1.659, respectively.
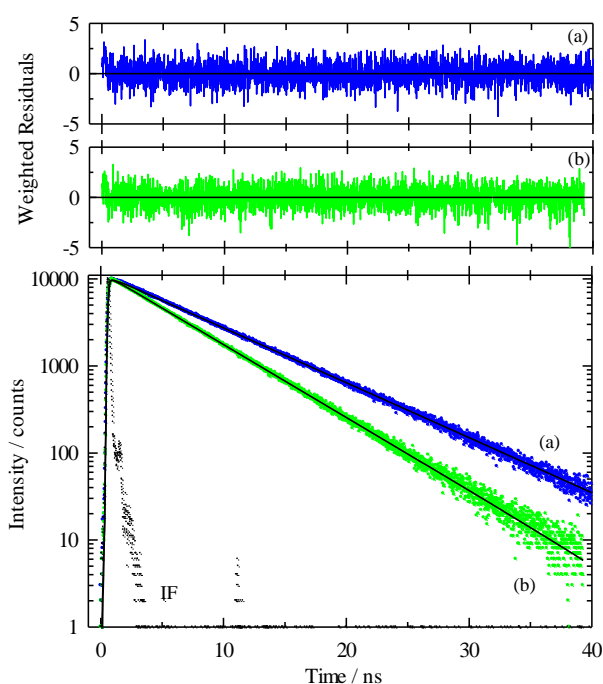
Figure 6. C153/scCO$_2$ intensity decays at 323 K; excitation was at 24,691 cm^{-1} with emission at 22,222 cm^{-1}. In the lower panel, dots are the measured decays and the solid lines are the resulting fits. The label "IF" shows the instrument response function. Blue trace "a" was at $\rho_r = 0.571$ and green trace "b" was at $\rho_r = 1.659$. The upper panels are the residuals to the sum-of-exponentials model with two time constants.
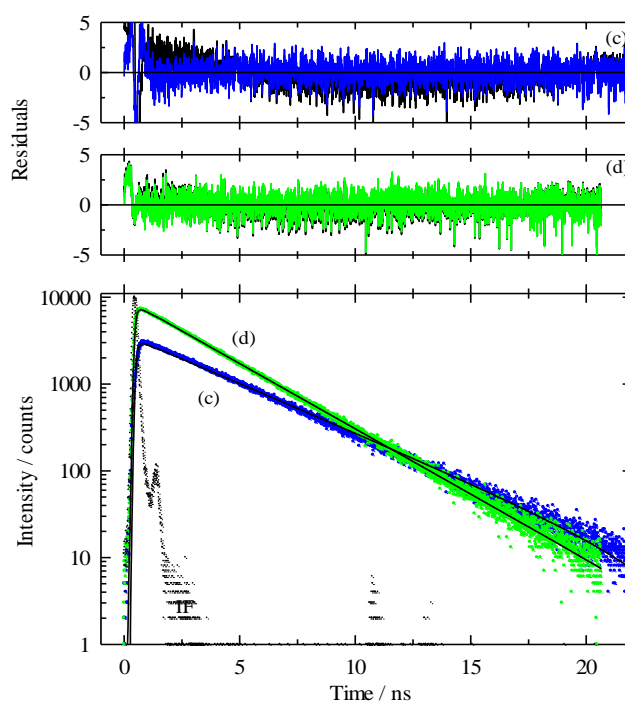

Figure 7. C153 intensity decays and subsequent fits in [P$_{6,6,6,14}$]$^+$ [Tf$_2$N]$^-$/scCO$_2$ at 323 K with excitation at 24,691 cm^{-1} and emission at 22,222 cm^{-1}. In the lower panel, dots are the measured decays and solid lines are the multi-exponential fits. The label "IF" shows the instrument response function. Blue trace "c" was measured at $\rho_r = 0.754$ and green trace "d" was at $\rho_r = 1.726$. The upper panels are the residuals to the sum-of-exponentials model with two time constants. Black lines are fits to a single exponential decay and colored lines are fits to a double exponential model.

Sample decays at $\rho_r = 0.754$ (blue trace "c") and $\rho_r = 1.726$ (green trace "d") for C153 in $[P_{6,6,6,14}]^+$ $[Tf_2N]^-/scCO_2$ are in Figure 7. Again, a sum-of-exponentials model was used to fit the decays with the shorter time constant used to account for scattered photons. The residuals show that at low density (Figure 7, panel (c)), a single time constant is not completely adequate to describe the intensity decay, whereas, at high density (Figure 7, panel (d)), there is very little difference between the one and the two component models. We noted improved fits were achieved by including a second time constant as evidenced by both the diminution of χ_r^2 and by increased randomness in the residuals and their autocorrelations (not shown). Comparing the neat $scCO_2$ and $IL/scCO_2$ traces, it is immediately clear that the C153 lifetime is significantly shorter in the presence of IL.

The complete set of fitting results are in Figure 8, and show the pre-exponential factors and excited-state lifetimes across the range of $scCO_2$ density for C153 in neat $scCO_2$ (open circles) and $[P_{6,6,6,14}]^+$ $[Tf_2N]^-/scCO_2$ (inverted triangles). The C153/$scCO_2$ results represent the monomer lifetime benchmark. Interestingly, for gas phase C153 a lifetime of ~7 ns is the expected value in the absence of any solute-solvent coupling [96], consistent with what might be expected in a low-density supercritical fluid. However, since prior steady-state measurements clearly indicated density augmentation in neat $scCO_2$ [28], lifetimes must also include the effects. Comparatively, when IL is included in the solution, two time constants yield the best fit to the decay data—the faster time constant accounts for scattered light (circles), and the slower time constant is the C153 lifetime (triangles). The fractional contributions for each time constant, upper panel of Figure 8, shows that the intensity decay is dominated by the 3–4 ns time constant. Three points are immediately apparent from these data. First, in low-density $IL/scCO_2$, the C153 excited-state lifetime was 3.9 ns, significantly less than the corresponding neat $scCO_2$ lifetime by more than 2 ns, which far exceeds the ± 70 ps uncertainty. As density was increased, the C153 lifetime decreased to 2.9 ns. We ascribe the diminution of lifetime across all densities to the presence of IL. McRae and Kasha discussed the effect of aggregation (dimerization) on dye emission and suggested that aggregation enhances the quantum yield for phosphorescence at the expense of that for fluorescence [97]. However, there are several parameters that directly influence dye behavior including intersystem crossing rates, aggregate geometry, and dye transition moment alignment. Thus, while dimerization might not contribute significantly to a reduced radiative rate through solute–solute coupling, it is not clear from our data whether this mode of decay is present. Second, we note the lack of additional time constants needed to fit the decay data such as would be expected for multiple emissive forms of C153, as we saw with the phosphonium chloride analog [57].

For $[P_{6,6,6,14}]^+$ $[Tf_2N]^-$, the anion is much more non-polar compared to chloride and we would expect more favorable interactions with $scCO_2$. At least from the perspective of lifetimes, it would appear that C153 may be less strongly driven to aggregate. Third, the intensity decays measured with emission set at 22,222 cm^{-1} (blue symbols) and 19,608 cm^{-1} (green symbols) are the identical to within-experimental uncertainty. Thus, these points from the intensity decay data do not appear to support or confirm the existence of C153 dimers, in contrast to the steady-state emission and anisotropy data. In an attempt to help reconcile this difference, we point out that the laser excitation does not uniquely excite the low energy peak at 19,608 cm^{-1} and reiterate that emission from the 22,222 cm^{-1} peak is always more intense as shown by the emission intensity ratio $I_{22222}/I_{19608} > 1$ across the density range. Therefore, any signal from the dimer at 19,608 cm^{-1} was never completely isolated. In fact, if both species were emitting simultaneously, the monomer signal would dominate, by at least up to four times the intensity over the density range studied here. At least from these data, it appears that in high-density $scCO_2$, solubilization is effective enough so that any C153 dimer formation (solute–solute aggregation) is negligible.
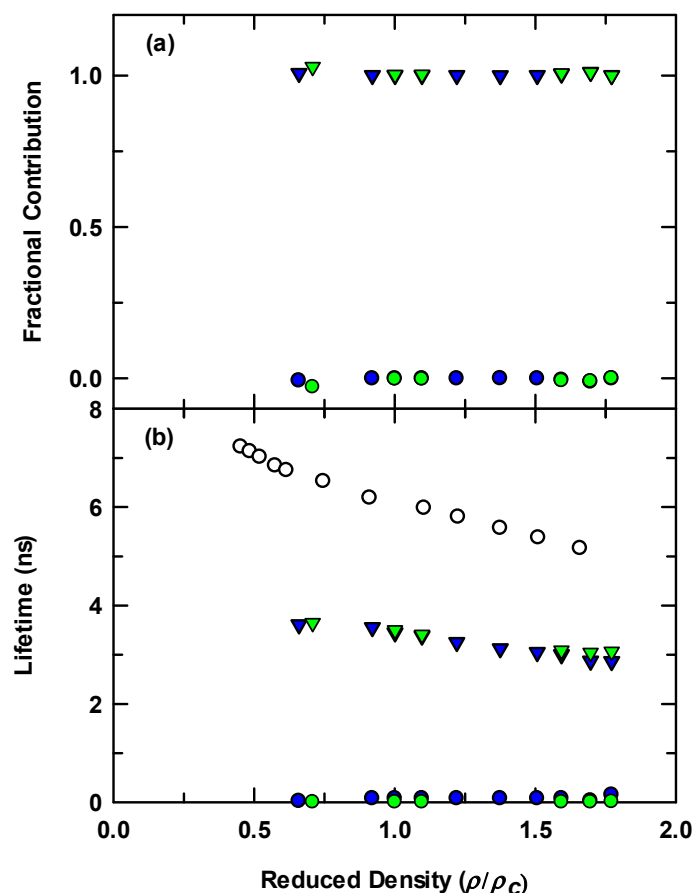
Figure 8. Decay parameters at 323 K for C153/$[P_{6,6,6,14}]^+$ $[Tf_2N]^-$/scCO$_2$ (blue and green filled symbols). Open circles in the lower panel are from the C153 fits in scCO$_2$ at 323 K. All IL data were acquired using excitation at 24,691 cm^{-1}, with emission at 22,222 cm^{-1} (blue symbols) and emission at 19,608 cm^{-1} (green symbols). Uncertainty is contained within the symbol size.

4. Summary and Conclusions

We have presented both steady-state and time-resolved fluorescence data for C153 in neat and IL-modified scCO$_2$ solutions. Our results suggest that the presence of trihexyltetradecylphosphonium bis(trifluoromethylsulfonyl)imide, $[P_{6,6,6,14}]^+$ $[Tf_2N]^-$, in these experiments influences the C153 spectroscopy. Evidence from excitation spectra of C153 in IL/scCO$_2$ solutions at $\rho_r < 1$ showed a large red shift and a significant change in spectral width (FWHM), features that both differed markedly compared to C153 in neat scCO$_2$ at 323K. Similarly, the emission of C153 in the IL/scCO$_2$ solution at $\rho_r < 1$ also showed large differences relative to the neat scCO$_2$ spectra that varied with choice of excitation wavelength. The most notable feature was observed when exciting at 22,222 cm^{-1} (= 450 nm), which isolated a clean emission peak at 19608 cm^{-1}. This peak was still discernable with higher energy excitation but the ability to differentiate the peak was rapidly lost as density was increased. Literature reports have demonstrated the formation of C153 dimers and discussed the observation of weak emission from H-aggregate formation [78,80,81]. This led us to hypothesize that we could possibly explain the seemingly anomalous C153 spectroscopy, at least in part, by invoking the presence of C153 aggregation when IL is included. We measured steady-state anisotropy that showed values approximately 1000-fold greater than the expected simple hydrodynamic response. The evaluation of potential contributions that might be responsible for the C153 response observed herein, including local density augmentation, C153 dimerization (aggregation), and the presence of IL and/or C153/IL aggregates in solution, led us to conclude that the observed effects suggest that IL influences our measurements. The recent demonstration of IL solubility in neat scCO$_2$ by Sivaraman and co-workers [92] provides

context against which we consider our spectroscopic data. Time-resolved fluorescence measurements showed two time constants, with the shorter component used to account for scattered light and the longer time associated with C153 lifetimes. Fractional contributions of the emission indicated that >99% of the intensity decay was associated with C153 emission. Lifetime data were inconclusive as to the presence of C153 dimers. However, the (essentially) exponential intensity decay yielded a time constant that was substantially shorter than measured for C153 alone in neat $scCO_2$.

In summary, while these measurements themselves cannot provide quantifying data on solution concentrations or molar ratios substantiating that IL is soluble in the $scCO_2$ phase, the composite data suggested that the presence of $[P_{6,6,6,14}]^+$ $[Tf_2N]^-$, among other contributions, does directly affect the C153 fluorescence. We further noted that the resulting supercritical fluid solution was optically transparent and single phased as judged by careful visual inspection at every pressure studied. As discussed, there is no spectral evidence for C153 aggregation in *neat* $scCO_2$ and so it appears from these data that the presence of IL somehow mediates the observed spectroscopy, particularly for $\rho_r < 1$. At $\rho_r > 1$, the solution behaves increasingly like that observed for C153 in neat $scCO_2$.

References

1. James, H.; Davis, J. Synthesis of Task-specific Ionic Liquids. In *Ionic Liquids in Synthesis*; Wasserscheid, P., Welton, T., Eds.; Wiley-VCH Verlag GmbH & Co KGaA: Weinheim, Germany, 2003; Volume 1, pp. 33–40.

2. Welton, T. Ionic liquids: A brief history. In *Electric Dipole Moments of the Fluorescent Probes Prodan and Laurdan: Experimental and Theoretical Evaluations*; Springer: Berlin, Germany, 2018; Volume 10, pp. 691–706. [CrossRef]

3. Zhou, Y.; Qu, J. Ionic Liquids as Lubricant Additives: A Review. *ACS Appl. Mater. Interfaces* **2017**, *9*, 3209–3222. [CrossRef] [PubMed]

4. MacFarlane, D.R.; Forsyth, M.; Howlett, P.C.; Kar, M.; Passerini, S.; Pringle, J.M.; Ohno, H.; Watanabe, M.; Yan, F.; Zheng, W.; et al. Ionic liquids and their solid-state analogues as materials for energy generation and storage. *Nat. Rev. Mater.* **2016**, *1*, 1–15. [CrossRef]

5. Perkin, S.; Kirchner, B.; Fayer, M.D. Preface: Special Topic on Chemical Physics of Ionic Liquids. *J. Chem. Phys.* **2018**, *148*, 193501. [CrossRef] [PubMed]

6. Gao, L.; Jiang, T.; Zhao, G.; Mu, T.; Wu, W.; Hou, Z.; Han, B. Transesterification between Isoamyl Acetate and Ethanol in Supercritical CO₂, Ionic Liquid, and Their Mixture. *J. Supercrit. Fluids* **2004**, *29*, 107–111. [CrossRef]

7. Shariati, A.; Peters, C.J. High-Pressure Phase Behavior of Systems with Ionic Liquids: II. The Binary System Carbon Dioxide+1-Ethyl-3-Methylimidazolium Hexafluorophosphate. *J. Supercrit. Fluids* **2004**, *29*, 43–48. [CrossRef]

8. Shariati, A.; Peters, C.J. High-Pressure Phase Behavior of Systems with Ionic Liquids: Part III. The Binary System Carbon Dioxide+1-hexyl-3-methylimidazolium hexafluorophosphate. *J. Supercrit. Fluids* **2004**, *30*, 139–144. [CrossRef]

9. Shariati, A.; Peters, C.J. High-Pressure Phase Behavior of Systems with Ionic Liquids: Measurements and Modeling of the Binary System Fluoroform+1-ethyl-3-methylimidazolium hexafluorophosphate. *J. Supercrit. Fluids* **2003**, *25*, 109–117. [CrossRef]

10. Batista, M.L.S.; Neves, C.M.S.S.; Carvalho, P.J.; Gani, R.; Coutinho, J.A.P. Chameleonic Behavior of Ionic Liquids and Its Impact on the Estimation of Solubility Parameters. *J. Phys. Chem. B* **2011**, *115*, 12879–12888. [CrossRef]

11. Jodry, J.J.; Mikami, K. New Chiral Imidazolium Ionic Liquids: 3D-network of Hydrogen Bonding. *Tetrahedron Lett.* **2004**, *45*, 4429–4431. [CrossRef]

12. Pollet, P.; Davey, E.A.; Urena-Benavides, E.E.; Eckert, C.A.; Liotta, C.L. Solvents for Sustainable Chemical Processes. *Green Chem.* **2014**, *16*, 1034–1055. [CrossRef]

13. Li, Z.; Xiao, Y.; Xue, W.; Yang, Q.; Zhong, C. Ionic Liquid/Metal–Organic Framework Composites for H2S Removal from Natural Gas: A Computational Exploration. *J. Phys. Chem. C* **2015**, *119*, 3674–3683. [CrossRef]

14. Ahmed, O.U.; Mjalli, F.S.; Gujarathi, A.M.; Al-Wahaibi, T.; Al-Wahaibi, Y.; AlNashef, I.M. Feasibility of Phosphonium-Based Ionic Liquids as Solvents for Extractive Desulfurization of Liquid Fuels. *Fluid Phase Equilibria* **2015**, *401*, 102–109. [CrossRef]

15. Zhou, Y.; Dyck, J.; Graham, T.W.; Luo, H.; Leonard, D.N.; Qu, J. Ionic Liquids Composed of Phosphonium Cations and Organophosphate, Carboxylate, and Sulfonate Anions as Lubricant Antiwear Additives. *Langmuir* **2014**, *30*, 13301–13311. [CrossRef] [PubMed]

16. Zakrewsky, M.; Lovejoy, K.S.; Kern, T.L.; Miller, T.E.; Le, V.; Nagy, A.; Goumas, A.M.; Iyer, R.S.; Del Sesto, R.E.; Koppisch, A.T.; et al. Ionic Liquids as a Class of Materials for Transdermal Delivery and Pathogen Neutralization. *Proc. Natl. Acad. Sci. USA* **2014**, *111*, 13313–13318. [CrossRef] [PubMed]

17. Cieszynska, A.; Wisniewski, M. Extraction of Palladium(II) from Chloride Solutions with Cyphos®IL 101/Toluene Mixtures as Novel Extractant. *Sep. Purif. Technol.* **2010**, *73*, 202–207. [CrossRef]

18. Kawano, R.; Matsui, H.; Matsuyama, C.; Sato, A.; Susan, M.A.B.H.; Tanabe, N.; Watanabe, M. High Performance Dye-Sensitized Solar Cells using Ionic Liquids as their Electrolytes. *J. Photochem. Photobiol. A* **2004**, *164*, 87–92. [CrossRef]

19. Sato, T.; Masuda, G.; Takagi, K. Electrochemical Properties of Novel Ionic Liquids for Electric Double Layer Capacitor Applications. *Electrochim. Acta* **2004**, *49*, 3603–3611. [CrossRef]

20. Zhao, G.; Jiang, T.; Han, B.; Li, Z.; Zhang, J.; Liu, Z.; He, J.; Wu, W. Electrochemical Reduction of Supercritical Carbon Dioxide in Ionic Liquid 1-n-Butyl-3-Methylimidazolium Hexafluorophosphate. *J. Supercrit. Fluids* **2004**, *32*, 287–291. [CrossRef]

21. Gui, J.; Cong, X.; Liu, D.; Zhang, X.; Hu, Z.; Sun, Z. Novel Brønsted acidic ionic liquid as efficient and reusable catalyst system for esterification. *Catal. Commun.* **2004**, *5*, 473–477. [CrossRef]

22. Wasserscheid, P.; Welton, T. *Ionic Liquids in Synthesis*; Wiley-VCH: Weinheim, Germany, 2003.

23. Fortunato, R.; González-Muñoz, M.J.; Kubasiewicz, M.; Luque, S.; Alvarez, J.R.; Afonso, C.A.M.; Coelhoso, I.M.; Crespo, J.G. Liquid Membranes using Ionic Liquids: The Influence of Water on Solute Transport. *J. Membr. Sci.* **2005**, *249*, 153–162. [CrossRef]

24. Scovazzo, P.; Kieft, J.; Finan, D.A.; Koval, C.; DuBois, D.; Noble, R. Gas Separations Using Non-Hexafluorophosphate [PF$_6$]$^-$ Anion Supported Ionic Liquid Membranes. *J. Membr. Sci.* **2004**, *238*, 57–63. [CrossRef]

25. Gruttadauria, M.; Riela, S.; Lo Meo, P.; D'Anna, F.; Noto, R. Supported Ionic Liquid Asymmetric Catalysis. A New Method for Chiral Catalysts Recycling. The Case of Proline-Catalyzed Aldol Reaction. *Tetrahedron Lett.* **2004**, *45*, 6113–6116. [CrossRef]

26. Ito, N.; Arzhantsev, S.; Heitz, M.; Maroncelli, M. Solvation Dynamics and Rotation of Coumarin 153 in Alkylphosphonium Ionic Liquids. *J. Phys. Chem. B* **2004**, *108*, 5771–5777. [CrossRef]

27. Kroon, M.C.; Peters, C.J. Supercritical Fluids in Ionic Liquids. In *Ionic Liquids Further UnCOILed*; John Wiley & Sons, Inc.: Hoboken, NJ, USA, 2014; pp. 39–57. [CrossRef]

28. Biswas, R.; Lewis, J.E.; Maroncelli, M. Electronic Spectral Shifts, Reorganization Energies, and Local Density Augmentation of Coumarin 153 in Supercritical Solvents. *Chem. Phys. Lett.* **1999**, *310*, 485–494. [CrossRef]

29. Beckman, E.J. Supercritical and near-critical CO$_2$ in green chemical synthesis and processing. *J. Supercrit. Fluids* **2004**, *28*, 121–191. [CrossRef]

30. Ploetz, E.A.; Smith, P.E. Gas or Liquid? The Supercritical Behavior of Pure Fluids. *J. Phys. Chem. B* **2019**, *123*, 6554–6563. [CrossRef]

31. Harrison, K.; Goveas, J.; Johnston, K.P.; O'Rear, E.A. Water-in-Carbon Dioxide Microemulsions with a Fluorocarbon-Hydrocarbon Hybrid Surfactant. *Langmuir* **1994**, *10*, 3536–3541. [CrossRef]

32. Iwai, Y.; Nagano, H.; Lee, G.S.; Uno, M.; Arai, Y. Measurement of Entrainer Effects of Water and Ethanol on Solubility of Caffeine in Supercritical Carbon Dioxide by FT-IR Spectroscopy. *J. Supercrit. Fluids* **2006**, *38*, 312–318. [CrossRef]

33. Li, A.; Tian, Z.; Yan, T.; Jiang, D.-E.; Dai, S. Anion-Functionalized Task-Specific Ionic Liquids: Molecular Origin of Change in Viscosity upon CO_2 Capture. *J. Phys. Chem. B* **2014**, *118*, 14880–14887. [CrossRef]

34. Bates, E.D.; Mayton, R.D.; Ntai, I.; Davis, J.H., Jr. CO_2 Capture by a Task-Specific Ionic Liquid. *J. Am. Chem. Soc.* **2002**, *124*, 926–927. [CrossRef]

35. Muldoon, M.J.; Aki, S.N.V.K.; Anderson, J.L.; Dixon, J.K.; Brennecke, J.F. Improving Carbon Dioxide Solubility in Ionic Liquids. *J. Phys. Chem. B* **2007**, *111*, 9001–9009. [CrossRef] [PubMed]

36. Lei, Z.; Dai, C.; Chen, B. Gas Solubility in Ionic Liquids. *Chem. Rev.* **2014**, *114*, 1289–1326. [CrossRef] [PubMed]

37. Vesna, N.-V.; Ana, S.; José, M.S.S.E.; Henrique, J.R.G.; Luis, P.N.R.; Manuel Nunes da, P. Multiphase Equilibrium in Mixtures of [C_4mim][PF_6] with Supercritical Carbon Dioxide, Water, and Ethanol: Applications in Catalysis. In *Ionic Liquids III A: Fundamentals, Progress, Challenges, and Opportunities*; American Chemical Society: Washington, DC, USA, 2005; Volume 901, pp. 301–310.

38. Shariati, A.; Peters, C.J. High-Pressure Phase Equilibria of Systems with Ionic Liquids. *J. Supercrit. Fluids* **2005**, *34*, 171–176. [CrossRef]

39. Kumełan, J.; Tuma, D.; Maurer, G. Simultaneous Solubility of Carbon Dioxide and Hydrogen in the Ionic Liquid [hmim][Tf2N]: Experimental Results and Correlation. *Fluid Phase Equilibria* **2011**, *311*, 9–16. [CrossRef]

40. Jang, S.; Cho, D.-W.; Im, T.; Kim, H. High-Pressure Phase Behavior of CO2+1-Butyl-3-Methylimidazolium Chloride System. *Fluid Phase Equilibria* **2010**, *299*, 216–221. [CrossRef]

41. Gutkowski, K.I.; Shariati, A.; Peters, C.J. High-pressure Phase Behavior of the Binary Ionic Liquid System 1-Octyl-3-methylimidazolium Tetrafluoroborate+Carbon Dioxide. *J. Supercrit. Fluids* **2006**, *39*, 187–191. [CrossRef]

42. Kroon, M.C.; Florusse, L.J.; Kühne, E.; Witkamp, G.-J.; Peters, C.J. Achievement of a Homogeneous Phase in Ternary Ionic Liquid/Carbon Dioxide/Organic Systems. *Ind. Eng. Chem. Res.* **2010**, *49*, 3474–3478. [CrossRef]

43. Mena, M.; Shirai, K.; Tecante, A.; Bárzana, E.; Gimeno, M. Enzymatic Syntheses of Linear and Hyperbranched Poly-l-Lactide Using Compressed R134a–Ionic Liquid Media. *J. Supercrit. Fluids* **2015**, *103*, 77–82. [CrossRef]

44. Timko, M.T.; Nicholson, B.F.; Steinfeld, J.I.; Smith, K.A.; Tester, J.W. Partition Coefficients of Organic Solutes between Supercritical Carbon Dioxide and Water: Experimental Measurements and Empirical Correlations. *J. Chem. Eng. Data* **2004**, *49*, 768–778. [CrossRef]

45. Andanson, J.-M.; Jutz, F.; Baiker, A. Investigation of Binary and Ternary Systems of Ionic Liquids with Water and/or Supercritical CO_2 by in Situ Attenuated Total Reflection Infrared Spectroscopy. *J. Phys. Chem. B* **2010**, *114*, 2111–2117. [CrossRef]

46. Tian, Q.; Li, R.; Sun, H.; Xue, Z.; Mu, T. Theoretical and Experimental Study on the Interaction Between 1-Butyl-3-Methylimidazolium Acetate and CO_2. *J. Mol. Liq.* **2015**, *208*, 259–268. [CrossRef]

47. Bhargava, B.L.; Balasubramanian, S. Insights into the Structure and Dynamics of a Room-Temperature Ionic Liquid: Ab Initio Molecular Dynamics Simulation Studies of 1-n-Butyl-3-methylimidazolium Hexafluorophosphate ([bmim][PF6]) and the [bmim][PF6]–CO_2 Mixture. *J. Phys. Chem. B* **2007**, *111*, 4477–4487. [CrossRef] [PubMed]

48. Kanakubo, M.; Makino, T.; Umecky, T.; Sakurai, M. Effect of Partial Pressure on CO_2 Solubility in Ionic Liquid Mixtures of 1-Butyl-3-methylimidazolium Acetate and 1-Butyl-3-methylimidazolium Bis(trifluoromethanesulfonyl)amide. *Fluid Phase Equilibria* **2016**, *420*, 74–82. [CrossRef]

49. Koller, T.M.; Heller, A.; Rausch, M.H.; Wasserscheid, P.; Economou, I.G.; Fröba, A.P. Mutual and Self-Diffusivities in Binary Mixtures of [EMIM][B(CN)4] with Dissolved Gases by Using Dynamic Light Scattering and Molecular Dynamics Simulations. *J. Phys. Chem. B* **2015**, *119*, 8583–8592. [CrossRef] [PubMed]

50. Lu, J.; Liotta, C.L.; Eckert, C.A. Spectroscopically Probing Microscopic Solvent Properties of Room-Temperature Ionic Liquids with the Addition of Carbon Dioxide. *J. Phys. Chem. A* **2003**, *107*, 3995–4000. [CrossRef]

51. Kumelan, J.; Tuma, D.; Maurer, G. Partial molar volumes of selected gases in some ionic liquids. *Fluid Phase Equilibria* **2009**, *275*, 132–144. [CrossRef]

52. Kim, J.E.; Lim, J.S.; Kang, J.W. Measurement and Correlation of Solubility of Carbon Dioxide in 1-Alkyl-3-Methylimidazolium Hexafluorophosphate Ionic Liquids. *Fluid Phase Equilibria* **2011**, *306*, 251–255. [CrossRef]

53. Blanchard, L.A.; Gu, Z.; Brennecke, J.F. High-Pressure Phase Behavior of Ionic Liquid/CO_2 Systems. *J. Phys. Chem. B* **2001**, *105*, 2437–2444. [CrossRef]

54. Afzal, W.; Liu, X.; Prausnitz, J.M. High Solubilities of Carbon Dioxide in Tetraalkyl Phosphonium-Based Ionic Liquids and the Effect of Diluents on Viscosity and Solubility. *J. Chem. Eng. Data* **2014**, *59*, 954–960. [CrossRef]

55. Carvalho, P.J.; Álvarez, V.H.; Marrucho, I.M.; Aznar, M.; Coutinho, J.A.P. High carbon dioxide solubilities in trihexyltetradecylphosphonium-based ionic liquids. *J. Supercrit. Fluids* **2010**, *52*, 258–265. [CrossRef]

56. Hutchings, J.W.; Fuller, K.L.; Heitz, M.P.; Hoffmann, M.M. Surprisingly High Solubility of the Ionic Liquid Trihexyltetradecylphosphonium Chloride in Dense Carbon Dioxide. *Green Chem.* **2005**, *7*, 475–478. [CrossRef]

57. Heitz, M.; Fuller, K.; Ordiway, K. Dissolution of Trihexyltetradecylphosphonium Chloride in Supercritical CO_2. *ChemEngineering* **2017**, *1*, 12. [CrossRef]

58. Johnston, K.P.; Harrison, K.L.; Clarke, M.J.; Howdle, S.M.; Heitz, M.P.; Bright, F.V.; Carlier, C.; Randolph, T.W. Water-in-Carbon Dioxide Microemulsions: An Environment for Hydrophiles Including Proteins. *Science* **1996**, *271*, 624–626. [CrossRef]

59. Heitz, M.P.; Carlier, C.; de Grazia, J.; Harrison, K.L.; Johnston, K.P.; Randolph, T.W.; Bright, F.V. Water Core Within Perfluoropolyether-Based Microemulsions Formed in Supercritical Carbon Dioxide. *J. Phys. Chem. B* **1997**, *101*, 6707–6714. [CrossRef]

60. Taek Lim, K.; Soo Hwang, H.; Sig Lee, M.; Dae Lee, G.; Hong, S.-S.; Johnston, K. Formation of TiO_2 Nanoparticles in Water-in-CO_2 Microemulsions. *Chem. Commun.* **2002**, 1528–1529. [CrossRef] [PubMed]

61. Lim, K.T.; Hwang, H.S.; Ryoo, W.; Johnston, K.P. Synthesis of TiO_2 Nanoparticles Utilizing Hydrated Reverse Micelles in CO_2. *Langmuir* **2004**, *20*, 2466–2471. [CrossRef]

62. Lewis, J.E.; Maroncelli, M. On the (Uninteresting) Dependence of the Absorption and Emission Transition Moments of Coumarin 153 on Solvent. *Chem. Phys. Lett.* **1998**, *282*, 197–203. [CrossRef]

63. Maroncelli, M.; Fleming, G.R. Picosecond solvation dynamics of coumarin 153: The importance of molecular aspects of solvation. *J. Chem. Phys.* **1987**, *86*, 6221–6239. [CrossRef]

64. Zhang, X.-X.; Breffke, J.; Ernsting, N.P.; Maroncelli, M. Observations of Probe Dependence of the Solvation Dynamics in Ionic Liquids. *Phys. Chem. Chem. Phys.* **2015**, *17*, 12949–12956. [CrossRef]

65. Becker, R.S.; Chakravorti, S.; Gartner, C.A.; de Graca Miguel, M. Photosensitizers: Comprehensive photophysics/photochemistry and theory of coumarins, chromones, their homologues and thione analogues. *J. Chem. Soc. Faraday Trans.* **1993**, *89*, 1007–1019. [CrossRef]

66. Natal'ya, A.K.; Oleg, L.K. The photochemistry of coumarins. *Photochem. Coumarins* **1992**, *61*, 683–696.

67. Reynolds, L.; Gardecki, J.A.; Frankland, S.J.V.; Horng, M.L.; Maroncelli, M. Dipole Solvation in Nondipolar Solvents: Experimental Studies of Reorganization Energies and Solvation Dynamics. *J. Phys. Chem.* **1996**, *100*, 10337–10354. [CrossRef]

68. Horng, M.L.; Gardecki, J.A.; Papazyan, A.; Maroncelli, M. Subpicosecond Measurements of Polar Solvation Dynamics: Coumarin 153 Revisited. *J. Phys. Chem.* **1995**, *99*, 17311–17337. [CrossRef]

69. Bradaric, C.J.; Downard, A.; Kennedy, C.; Robertson, A.J.; Zhou, Y. Industrial Preparation of Phosphonium Ionic Liquids. *Green Chem.* **2003**, *5*, 143–152. [CrossRef]

70. Lemmon, E.W.; McLinden, M.O.; Friend, D.G. Thermophysical Properties of Fluid Systems. In *NIST Chemistry WebBook, NIST Standard Reference Database Number 69*; Linstrom, P.J., Mallard, W.G., Eds.; National Institute of Standards and Technology: Gaithersburg, MD, USA, 1998. Available online: http://webbook.nist.gov (accessed on 19 September 2019).

71. Span, R.; Wagner, W. A New Equation of State for Carbon Dioxide Covering the Fluid Region from the Triple-Point Temperature to 1100 K at Pressures up to 800 MPa. *J. Phys. Chem. Ref. Data* **1996**, *25*, 1509–1596. [CrossRef]

72. Barra, K.M.; Sabatini, R.P.; McAtee, Z.P.; Heitz, M.P. Solvation and Rotation Dynamics in the Trihexyl(tetradecyl)phosphonium Chloride Ionic Liquid/Methanol Cosolvent System. *J. Phys. Chem. B* **2014**, *118*, 12979–12992. [CrossRef]

73. O'Connor, D.V.; Phillips, D. *Time-Correlated Single Photon Counting*; Academic Press: Cambridge, MA, USA, 1984.

74. Becker, W. *Advanced Time-Correlated Single Photon Counting Techniques*; Springer: Berlin/Heidelberg, Germany, 2005. [CrossRef]

75. Lakowicz, J.R. *Principles of Fluorescence Spectroscopy*; Springer: New York, NY, USA, 2006. [CrossRef]

76. Hoffmann, M.M.; Heitz, M.P.; Carr, J.B.; Tubbs, J.D. Surfactants in Green Solvent Systems—Current and Future Research Directions. *J. Dispers. Sci. Technol.* **2003**, *24*, 155–171. [CrossRef]

77. Holmes, J.D.; Ziegler, K.J.; Audriani, M.; Lee, C.T., Jr.; Bhargave, P.A.; Steytler, D.C.; Johnston, K.P. Buffering the Aqueous Phase pH in Water-in-CO_2 Microemulsions. *J. Phys. Chem. B* **1999**, *103*, 5703–5711. [CrossRef]

78. Verma, P.; Pal, H. Aggregation Studies of Dipolar Coumarin−153 Dye in Polar Solvents: A Photophysical Study. *J. Phys. Chem. A* **2014**, *118*, 6950–6964. [CrossRef]

79. Sen, T.; Bhattacharyya, S.; Mandal, S.; Patra, A. Spectroscopic Investigations on the H-Type Aggregation of Coumarin 153 Dye Molecules: Role of Au Nanoparticles and γ-Cyclodextrin. *J. Fluoresc.* **2012**, *22*, 303–310. [CrossRef]

80. Verma, P.; Pal, H. Intriguing H-Aggregate and H-Dimer Formation of Coumarin-481 Dye in Aqueous Solution As Evidenced from Photophysical Studies. *J. Phys. Chem. A* **2012**, *116*, 4473–4484. [CrossRef] [PubMed]

81. Verma, P.; Pal, H. Unusual H-Type Aggregation of Coumarin-481 Dye in Polar Organic Solvents. *J. Phys. Chem. A* **2013**, *117*, 12409–12418. [CrossRef] [PubMed]

82. Lee, D.; Greenman, L.; Sarovar, M.; Whaley, K.B. Ab Initio Calculation of Molecular Aggregation Effects: A Coumarin-343 Case Study. *J. Phys. Chem. A* **2013**, *117*, 11072–11085. [CrossRef] [PubMed]

83. Liu, X.; Cole, J.M.; Low, K.S. Molecular Origins of Dye Aggregation and Complex Formation Effects in Coumarin 343. *J. Phys. Chem. C* **2013**, *117*, 14723–14730. [CrossRef]

84. Kasha, M.; Rawls, H.R.; El-Bayoumi, M.A. The Exciton Model in Molecular Spectroscopy. *Pure Appl. Chem.* **1965**, *11*, 371–392. [CrossRef]

85. Kasha, M. Energy Transfer Mechanisms and the Molecular Exciton Model for Molecular Aggregates. *Radiat. Res.* **1963**, *20*, 55–70. [CrossRef]

86. Minami, K.; Aizawa, T.; Kanakubo, M.; Hiejima, Y.; Nanjo, H.; Smith, J.; Richard, L. Local Density Augmentation of Excited 1-(dimethylamino)naphthalene in Supercritical Water. *J. Supercrit. Fluids* **2006**, *39*, 206–210. [CrossRef]

87. Ruckenstein, E.; Shulgin, I.L. Why Density Augmentation Occurs in Dilute Supercritical Solutions. *Chem. Phys. Lett.* **2000**, *330*, 551–557. [CrossRef]

88. Ingrosso, F.; Ladanyi, B.M.; Mennucci, B.; Scalmani, G. Solvation of Coumarin 153 in Supercritical Fluoroform. *J. Phys. Chem. B* **2006**, *110*, 4953–4962. [CrossRef]

89. Heitz, M.P.; Maroncelli, M. Rotation of Aromatic Solutes in Supercritical CO_2: Are Rotation Times Anomalously Slow in the Near Critical Regime? *J. Phys. Chem. A* **1997**, *101*, 5852–5868. [CrossRef]

90. Perrin, F. Polarisation de la lumière de fluorescence. Vie moyenne des molécules dans l'etat excité. *J. Phys. Radium* **1926**, *7*, 390–401. [CrossRef]

91. Horng, M.-L.; Gardecki, J.A.; Maroncelli, M. Rotational Dynamics of Coumarin 153: Time-Dependent Friction, Dielectric Friction, and Other Nonhydrodynamic Effects. *J. Phys. Chem. A* **1997**, *101*, 1030–1047. [CrossRef]

92. Pitchaiah, K.C.; Lamba, N.; Sivaraman, N.; Madras, G. Solubility of trioctylmethylammonium chloride in supercritical carbon dioxide and the influence of co-solvents on the solubility behavior. *J. Supercrit. Fluids* **2018**, *138*, 102–114. [CrossRef]

93. Guo, W.; Li, Z.; Fung, B.M.; O'Rear, E.A.; Harwell, J.H. Hybrid surfactants containing separate hydrocarbon and fluorocarbon chains. *J. Phys. Chem.* **1992**, *96*, 6738–6742. [CrossRef]

94. Guo, W.; Fung, B.M.; O'Rear, E.A. Exchange of hybrid surfactant molecules between monomers and micelles. *J. Phys. Chem.* **1992**, *96*, 10068–10074. [CrossRef]

95. Birks, J.B. *Photophysics of Aromatic Molecules*; Wiley-Interscience: Hoboken, NJ, USA, 1970.

96. Jin, H.; Baker, G.A.; Arzhantsev, S.; Dong, J.; Maroncelli, M. Solvation and Rotational Dynamics of Coumarin 153 in Ionic Liquids: Comparisons to Conventional Solvents. *J. Phys. Chem. B* **2007**, *111*, 7291–7302. [CrossRef]

97. McRae, E.G.; Kasha, M. Enhancement of Phosphorescence Ability upon Aggregation of Dye Molecules. *J. Chem. Phys.* **1958**, *28*, 721–722. [CrossRef]